This is a repository copy of *Investigation of wrinkling failure mechanics in metal spinning by Box-Behnken design of experiments using finite element method*.

White Rose Research Online URL for this paper:
http://eprints.whiterose.ac.uk/89693/

Version: Accepted Version

Investigation of Wrinkling Failure Mechanics in Metal Spinning by Box-Behnken Design of Experiments using Finite Element Method

M. Watson, H. Long[*] and B. Lu

Department of Mechanical Engineering, The University of Sheffield, Sheffield, S1 3JD, UK

* Corresponding author:
E-mail address: h.long@sheffield.ac.uk

Abstract

An investigation into material wrinkling failure mechanics of conventional metal spinning and the effects of process parameters and material properties are presented in this paper. By developing finite element (FE) models using the Box-Behnken Design of Experiments, the effects of six key process and material parameters on the start of material wrinkling have been investigated. These key factors include roller feed per pass, feed rate, thickness, tool path profile, Young's modulus, Yield stress and strain hardening exponent. The results of FE simulation are validated by comparing the modelled roller tool forces and spun part end shape with that measured during a spinning experiment.

From FE simulations, large residual stresses in the form of bending moments are found to be present in the flange of the blank, induced by the roller contact. It is found that material wrinkling failure begins when a plastic hinge is formed between the roller and the edge of the blank. It is found that both roller feed per pass and feed rate produce the most significant effect on the initiation of wrinkling failure as they increase the bending stresses causing a plastic hinge to form more rapidly thus wrinkling to occur more quickly.

Key words:
Conventional metal spinning; wrinkling failure; Box-Behnken design of experiments; Finite Element method;

1. Introduction

Metal spinning in modern times has been widely used in various industries requiring high precision material processing, some examples of spun parts including aero engine inlet rings, pressure vessel, large bearing rings for wind turbines, and jet-engine nose cones. As one of the near-net shape forming processes, sheet metal spinning involves the feeding motion of one or more rollers against a metal sheet rotating together with the main spindle of a machine to obtain desired geometries by inducing continuous and localized plastic deformation on the sheet, as shown in **Fig. 1**. Due to the nature of localized material deformation, this process has inherent advantages, such as low forming loads, simple tooling, good dimensional accuracy, high material utilization, low production costs and improved mechanical properties, be apt to obtain lightweight parts with flexibility in manufacturing [1].

Wrinkling is one of three material processing failures commonly observed in the sheet metal spinning [2-4]. Before Finite Element (FE) analysis was first used to simulate the metal spinning process the stress state in the forming region was accepted to be as shown in **Fig. 1** [2]. Contrary to this several FE models have found that in the roller contact area the metal blank is subject to local bending. Sebastani et al. [5], Wang and Long [6] noted that only a small portion of the unsupported flange was under compressive tangential stresses. They noted that a toothed stress pattern appeared in the flange; however this could not be shown as a pre-state to

wrinkling failure [5-6]. Instead, wrinkling occurred if the area of high compressive tangential stress in the flange did not "recover" to a tensile tangential stress when the roller contact moved away. Music and Allwood [7] however identified two separate modes of wrinkling failure: the first is similar to the one identified above and the second happens later in the process and is more similar to wrinkling in deep drawing.

It is generally accepted that wrinkling in the flange is a sheet buckling phenomenon, first proposed by Senior [8] and Kobayashi [9]. This is based on the assumption that compressive stresses along the circumference direction of the sheet are induced due to the action of the roller, as illustrated in **Fig. 1**. Senior [8] identified that the energy method was a possible method for predicting the sheet buckling failure, whereby a defected shape was assumed and the potential energy relating to this defection was evaluated. The critical condition was given when the total energy to restore equilibrium was equal to that of the forces which produced the defection. This was the method used by Senior [8] to develop the instability theory for deep drawing and was later adapted by Kobayashi [9] for metal spinning. However this method may not be accurate due to Senior [8] neglecting the radial stress in the blank and the static condition imposed by use of the energy method.
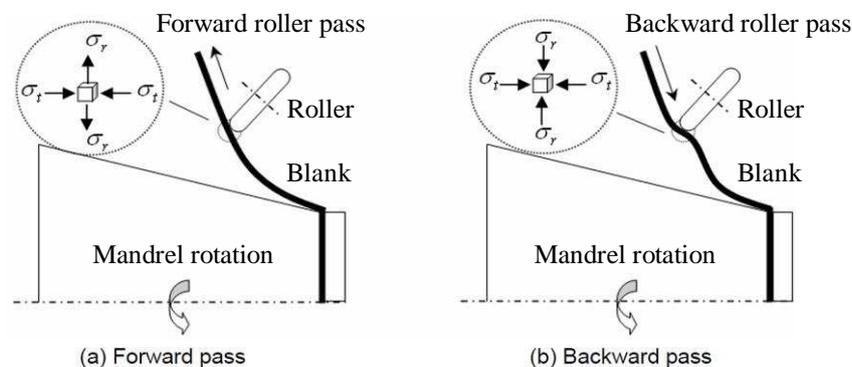
Fig. 1 Theoretical stress distributions of the forming region during spinning [6]

Most of the experimental investigations on material failures focused on shear forming rather than conventional spinning. The failure studies in the shear forming have been carried out by investigating the spinnability, which was first mentioned by Kegg [10] as the ability of metal blank to undergo shear forming without fracture. Hayama and Tago [11] further refined the term of spinnability as the ability of a sheet metal to undergo deformation by shear forming without the wrinkles in the flange and no fractures on the blank wall. Most recently, Kawai et al. [12] conducted spinnability studies of "die-less" shear forming of both conical and hemispherical parts by using a cylindrical mandrel.

To investigate the initiation of material wrinkling, Hayama et al. [13] measured the radial and circumferential strains as well as the periodic variations of curvatures on the flange, by attaching strain gauges on both sides of the flange before spinning. In a later study, Hayama [14] used the sudden change of the vibration of the axial force, the feeding force, to determine the exact moment when the wrinkling occurred in the shear forming. Arai [15] used a laser sensor to measure the flange wrinkles and a force transducer to measure the tool forces in a shear forming process, concluded that the fluctuations of tool forces could be used to detect the initiation of wrinkling failures.

While some experimental studies focusing on wrinkling failure in shear forming have been completed only few has been found concerning conventional metal spinning. Limited spinability studies were conducted using a single pass process by Xia et al [16]. This was supported by the results produced by Essa and Hartley [17], who carried out FE simulation based on Xia et al. experimental work. An experimental study on wrinkling was performed and it concluded that the tool force increased when wrinkling occurs and this

increase was dependent on the blank material [18]. Kleiner et al. [19] studied the evolution of wrinkles during the first pass of conventional spinning. They observed that the wrinkles progressed with the roller movement and divided the wrinkling into 5 stages. They found that at the onset a single wrinkle existed under the roller and after the first complete revolution the wrinkles grew in aptitude with subsequent revolutions. They concluded that the wrinkling was not only caused by static buckling but also influenced or even triggered by the dynamic effects from the feeding of roller and the rotation of the blank.

The effect of process parameters on wrinkling in the conventional spinning and shear forming have been studied in few reported work. Kleiner et al [19] reported that the diameter and thickness of the blank had the most significant effect on the wrinkling failure in the conventional spinning. Hayama et al [14] reported that the feed ratio, thickness and diameter of the blank were very important factors for the wrinkling in shear forming process. Wang and Long [20] developed the feed ratio limit diagram based on FE simulations to predict wrinkling failure in conventional spinning. The authors also studied effects of roller path profiles and tool compensation on wrinkling by conducting both FE simulation and experimental validation [21]. In general, if reducing the blank thickness or increasing the feed ratio and sheet diameter the possibility of wrinkling failures will increase accordingly [18]. Further investigation is needed to develop an in-depth understanding of wrinkling failure mechanics thus to develop an accurate method to predict the occurrence of wrinkling in metal spinning.

In this paper, an investigation into wrinkling failure mechanics of conventional metal spinning and the effect of process parameters is presented. By developing finite element models using Box-Behnken Design of Experiments, the effects of six key process and material parameters on the start of material wrinkling has been investigated. These key parameters include roller feed per pass, feed rate, thickness, tool path profile, Young's modulus, Yield stress and strain hardening exponent. The results of FE simulation are validated by comparing the modelled roller forces and spun part end shape with that measured during a spinning experiment. From FE simulation, large residual stresses in the form of bending moments are found to be present in the flange, induced by the roller contact. It is found that wrinkling failure begins when a plastic hinge is formed between the roller and the edge of the blank. These bending moments cause the wrinkled state of the flange to be energetically favourable, which is seen as a reduction in the magnitude of these moments and the elastic strain energy of the FE model at the point of wrinkling. The shape of the ideal involute roller path for the first pass of conventional spinning has been investigated and an angle of 40 degrees has been found to be optimum for the first pass to prevent wrinkling failure. It was found that both roller feed per pass and feed rate produced the most significant effect in the initiation of wrinkling failure as they increased the bending stresses causing a plastic hinge to form more rapidly thus wrinkling to occur more quickly.

2. Development of Finite Element Models

2.1 Selection of simulation algorithm

The metal spinning process contains non-linearity in the contact boundary conditions, the plastic flow of the work piece and the large deformation of geometry. Instabilities such as material wrinkling failure can also cause convergence problems if dynamic implicit solution methods are used. By contrast the small time steps and linear approximation used by explicit formulations can cope well with non-linearity because displacements are calculated without reference to the end time state. The explicit method approximates the system to be linear to determine the properties of the system for each time interval. Because of this the stable time increment of the analysis is very small. The maximum stable time increment, δ_t, for an explicit model is given by the Courant condition, which is proportional to a characteristic length of the smallest element, L_e, and the square root of the density of the material used, ρ, as shown below:

$$\delta_t = \frac{L_e}{c} \propto \frac{L_e \sqrt{\rho}}{\sqrt{E}} \tag{1}$$

It is clear that the maximum stable time increment can be increased by artificially increasing the density of the material; this is known as mass scaling. The overall solution time can also be reduced by applying forces and displacements more quickly; this is known as load rate scaling. As shown in Equation (1), mass scaling reduces the simulation time by the square root of the mass scaling factor. Load rate scaling however produces a linear increase in simulation speed by reducing the spinning process time. Because of this it has been concluded by Hamilton and Long [22] that load rate scaling is more appropriate for simulating the spinning process if no rate dependency of the material is taken into consideration. However, if the scaling factor used is too high, the corresponding inertial forces will affect the mechanical response and produce unrealistic dynamic effect. Therefore the scaling factor should be carefully selected [6]. The commercial software ABAQUS Explicit is used in this study.

2.2 Spinning process setup and modelling

The spinning process set up used in the FE simulation is shown in **Fig. 2**, similar to that used in the experimental testing of spinning force measurement reported by Long et al. [18]. The back plate and roller are modelled as analytical rigid bodies leaving the blank as the only deformable body in the simulation. The blank is meshed with 8 node hexahedral continuum shell elements with enhanced hourglass control and reduced integration to relive shear locking. The central portion of the blank, where it is clamped against the back plate, is neglected in order to improve the computational efficiency. The domain parallelization is used in this study as it typically produces a larger speed up and scales better with more processors.

The penalty contact algorithm is used in the FE simulation, which has been used successfully in many previous models as reported in the literature [6, 21, 23-24]. The coulomb friction coefficients of contact surfaces are defined as back plate to blank 0.3, mandrel to blank 0.3, and roller to blank 0.35 where the degree of freedom of the roller is allowed for by boundary conditions set in the local coordinate system of the roller and a more realistic friction coefficient has been selected. The spinning process has been split into 3 steps to allow the boundary conditions of the FE model to change as they would during the actual spinning process. These steps are: clamping the blank in place, beginning rotation of the blank, and forming the blank by the action of the roller.
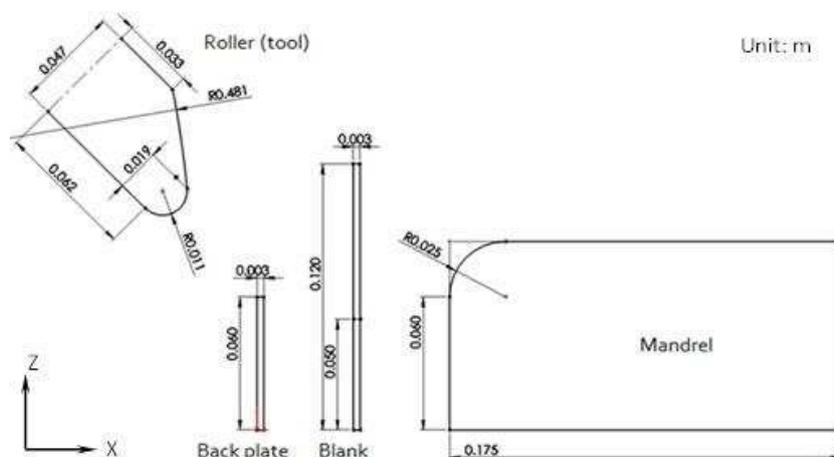
Fig. 2 Illustration of spinning process set up

In order to gain a more generalised understanding of the effect of the material properties on the mechanics of wrinkling failure in the blank, materials will be modelled in terms of a Young's modulus, yield stress and strain hardening exponent. These are related to the strain by Equation 2. The use of this equation forces a definite yield point in the material model. Because of this the validation case and hence the focus of this study will be on steel like materials.

$$\sigma = \begin{cases} E\epsilon, & \epsilon \leq \dfrac{\sigma_E}{E}, \\ \sigma_E \left(\dfrac{E\epsilon}{\sigma_E}\right)^n, & \epsilon \geq \dfrac{\sigma_E}{E}. \end{cases}$$

(2)
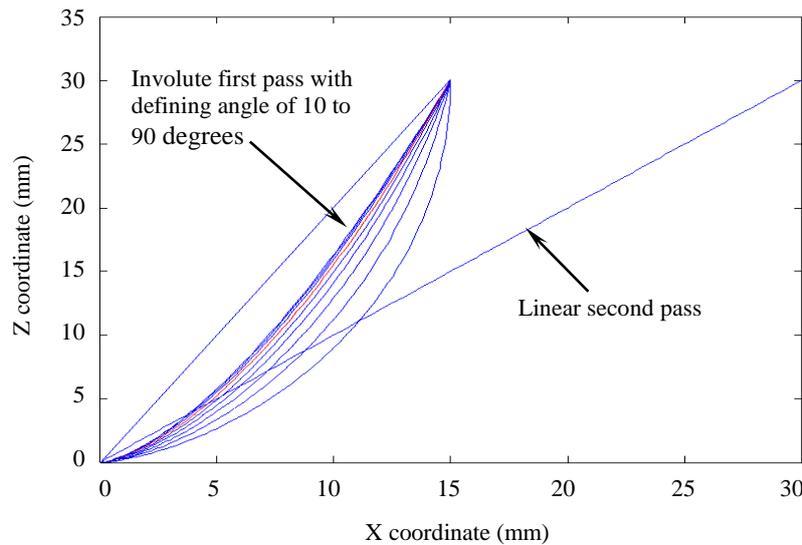
Fig. 3 Involute roller paths used in FE simulations

The roller path used for the study was an involute path described by 100 points per pass found using Equations 3. An involute path was chosen as this has been shown to produce the lowest stresses in the work piece [18, 21, 25]. The path was scaled to fit the diameter of the blank and the required feed rate. The timing of this path was controlled to give a constant feed rate in the axial direction of the roller. Graphs of the involute path used in the FE models to find an optimum roller pass are shown in **Fig. 3**, where the path is defined by the x- and z-coordinate as given in **Fig. 3**. The start point of the path was chosen to ensure that the path did not force compression of the blank between the roller and the mandrel. The defining angle of an involute path controls the curvature of the roller path; an angle of 0 degree would be a straight line as shown in **Fig. 3**. In order to optimise the defining angle for an involute path, 9 models were created with defining angles of 10 to 90 degrees for their first pass and a linear second pass is used as shown in **Fig. 3**.

$$x = a(\cos t + t \sin t)$$
$$y = a(\sin t - t \cos t)$$

(3)

3. Box-Behnken Design of Experiments

This study considers three process parameters and three material properties using the Design of Experiments (DOE) to investigate which factors are the most important with regards to the occurrence of material wrinkling failure and why they have this effect. The three process parameters are the roller feed per pass, feed rate and thickness of the blank, the material properties are Young's modulus, yield stress and strain hardening exponent. A typical value of each parameter is selected based on previous work of the authors, Wang and Long [6, 18, 21, 25] and it is decided that each parameter should be allowed to vary by the same

percentage of its typical value. A Box-Behnken design is used to investigate the process parameters and material properties on wrinkling as this reduces the number of computational experiments needed while ensuring the maximum possible information about the system response can be gained. **Fig. 4** compares a three-variable full factorial design with the Box-Behnken design geometrically, where the number of experimental runs is reduced from $3^3 = 27$ to 13 runs. The Box-Behnken design is a spherical design, with all points lying on a sphere of radius of $\sqrt{2}$. It does not contain any points on the vertices of the cubic region created by the upper and lower limits of each variable. For six variables used in this study, the number of experiments is reduced from $6^3 = 216$ in the full factorial design to 49 in the Box-Behnken design.

(a) Full Factorial Design   (b) Box-Behnken Design
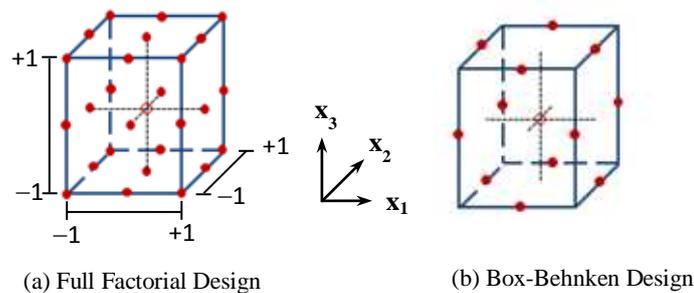
Fig. 4 Illustration of design of experiments for three variables

Several test cases using FE models were run and a setup of process parameters was devised in which all models would fail by wrinkling during the simulation of spinning process. The maximum percentage of variation of the variables that could be tolerated to achieve this scheme was 15%. The typical values for the material properties were chosen to be close to those of the material used in the experimental study which will be used in the validation of FE models. The typical values for the process parameters were chosen to enforce the scheme described above. The typical values as well as the maximum and minimum values used for each of the parameters are shown in Table 1.

In total 49 runs of parameter variations using the Box-Benhnken DOE were created as part of this analysis, a full list of models is provided in Appendix 1. Run number 49 contained the typical values of process and material parameters. The Matlab codes were created to generate the changing variables for each parameter considered in 49 runs. The python codes were produced to create the 49 FE models and execute the FE simulations and data analysis automatically.

Table 1 Parameters used in the Box Behnken Design of Experiments

	Feed per pass (mm)	Feed rate (mm/s)	Blank thickness (mm)	Young's Modulus (MPa)	Yield stress (MPa)	Strain hardening exponent
Min value	10.625	5.1	1.19	151 470	212.5	0.0663
Mid value	12.5	6	1.4	178 200	250	0.078
Max value	14.375	6.9	1.61	204 930	287.5	0.0895

4. Validation of Finite Element Models

4.1 Comparison of FE modelled roller forces with experimental measurement

The FE model developed is validated by comparing the simulated roller forces with that measured in an experimental testing. In the experimental testing spinning roller forces in three orthogonal directions, radial, axial and tangential, are obtained using a Kistler piezoelectric force transducer [24]. These force components

are defined as $F_{Axial, Local}$, $F_{Radial, Local}$ and $F_{Tangential, Local}$, as shown in **Fig. 5a**. The measured axial and radial force components in the local coordinates are then resolved into the global coordinate system (X, Y, and Z). The three global force components are defined as F_{Axial}, F_{Radial} and $F_{Tangential}$, which are used in the tool force comparison and analysis. The blank material used is mild steel with a diameter of 240 mm and thickness of 1.2 mm. The dimensions of the roller and mandrel are given in Wang and Long [6]. Three forward roller passes were used where the feed rate of 13.3 mm/s and a rotational speed of 550 rpm were used in the experiment.

As shown in **Fig. 5b**, the tool force history clearly consists of three forward passes. Throughout the spinning process, the axial force component is the greatest followed by the radial force, and the tangential force is the smallest. This is in good agreement with that obtained by Wang *et al.* [26]. The peak values of axial and radial forces increase with the progress of the spinning process and the maximum axial and radial force values occur at the 3rd pass correlated to the design of the specific roller passes in this experiment.

A FE model is created according to the details of the experiment for the purpose of validation. **Fig. 6** shows the comparison of the axial roller force time history during the first roller path between the FE model and experiment. As can be seen the FE results are in good agreement with the experimental results with an error of only 11.3% for the maximum value of the axial roller force. For this reason the FE simulation is thought to perform accurately.
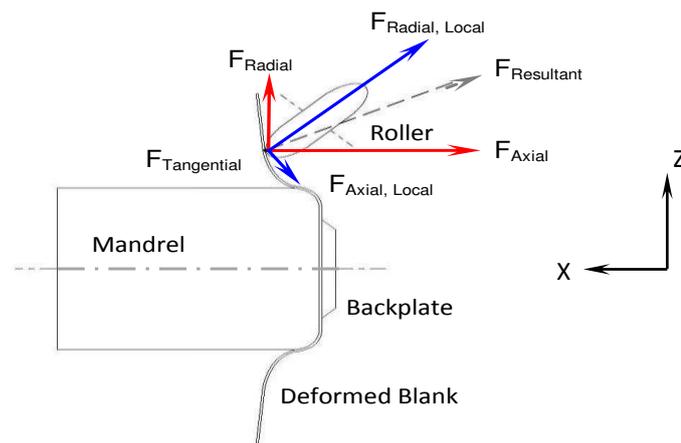
(a) Definition of local and global roller force components
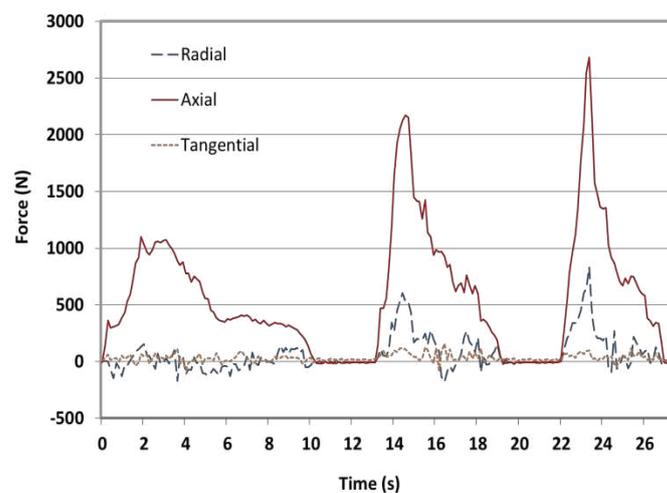
(b) Measured radial, axial and tangential force components using three roller passes

Fig. 5 Measured roller force components in a spinning experiment
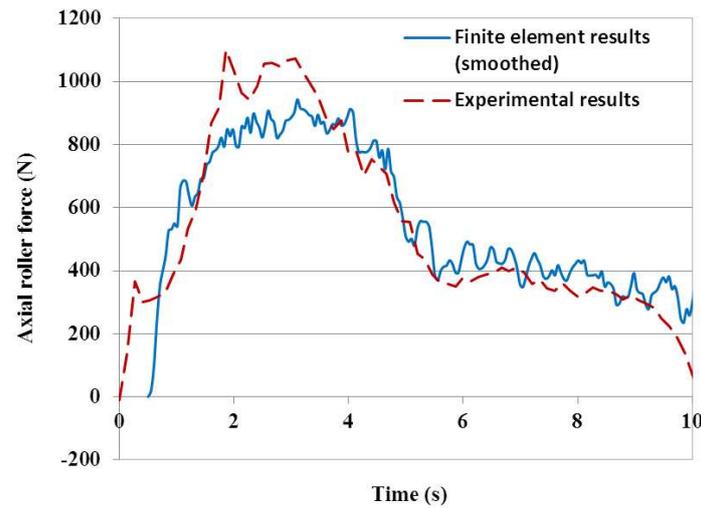
Fig. 6 Comparison of axial roller force of the first pass obtained from FE simulation and experiment

4.2 Finite Element mesh refinement and convergence study

FE models using 90, 120, 180, 200 elements around the circumference and 5, 7, 9, 11 integration points through the thickness of the continuum shell elements have been used to investigate the convergence to achieving required simulation accuracy. Both the shape form and magnitude of the roller force time history are checked and the results are shown in Table 2. Each model is solved across 3 cores running at 3.3GHz on a machine with 16 GB of RAM running at 1600MHz. Solution times vary between 7 and 27 hours depending on the number of elements in the model and to a lesser extent the number of integration points used.

As suggested by Long et al. [24] the continuum shell elements predisposition to wrinkling has been observed as the most coarsely meshed Models 1~3 wrinkled unrealistically. Also, in agreement with the literature, it has been observed that the effect of a coarse mesh is to stiffen the blank. These effects are only present in the most unrefined meshes and disappear from Model 4 onwards where the number of elements around the circumference exceeds 90. It has also been observed that using several continuum shell elements in the thickness direction can lead to discontinuous stress as in Model 5. It should also be noted that the shape of the roller force plot for the more refined meshes is in much better agreement with the experimental results. Table 2 shows that the changes in the maximum force are relatively small for changes above 180 elements around the circumference and 9 integration points through the thickness, thus the mesh is considered to have converged at this value. Because of this for the remaining work the mesh of Model 8 will be used.

Table 2 Results of the mesh refinement study

Model	Elements in circumference	Elements in thickness	Number of elements	Integration points in thickness	Maximum axial roller force (N)	Model validation with experiment
1	90	1	2552	5	992.8	Unrealistically wrinkled
2	90	2	5098	5	1001.3	Unrealistically wrinkled
3	90	3	7644	5	1004.0	Unrealistically wrinkled
4	120	1	3135	5	912.4	Part end shape agrees with Exp.
5	120	2	6264	5	940.9	Discontinuous stress
6	180	1	4631	5	808.3	Part end shape agrees with Exp.
7	180	1	4631	7	831.8	Part end shape agrees with Exp.
8	**180**	**1**	**4631**	**9**	**897.9**	**Force and part end shape agree with Exp.**
9	200	1	5000	9	903.7	Force and part end shape agree with Exp.
10	180	1	4631	11	904.2	Force and part end shape agree with Exp.

5. Results and Discussion

5.1 Global stress distribution

The maximum in-plane principal stresses of the top and bottom surface of the blank are shown in **Fig. 7**. Zone A includes an area of high stress due to the blank being bent over the mandrel, resulting tensile stress on the top surface and compressive stress on the bottom surface. The tool contact is in a region (B) of high compressive stress on the top and tensile stress on the bottom and is responsible for the spiral pattern of stress visible in region C. The spiral region appears not only to be under equivalent tension state as previously thought [5] but also subject to bending stresses (D) with the top surface subject to high tangential tension and the lower surface in tangential compression. This is a consequence of the shape that the blank is being formed into. The top and bottom surfaces of the blank are originally equal but end with one surface compressed to become the inner surface of the spun part and the other stretched to form the outer surface.

Another region of bending exists as indicated by region E on **Fig. 7 (c)**. This region is bending in resistance to the deformation of the roller, however it is bending upwards. This can be visualised if the entire blank is thought to be to some extent pivoting around its contact with the mandrel at point A. Examination of the von Mises results for the bottom surface indicates that this area is yielding. This presents another mechanism for circumferential cracking as this area of the blank is under bending stresses which regularly reverse as the blank rotates.

(a) Wrinkling modelling   (b) Top surface   (c) Bottom surface
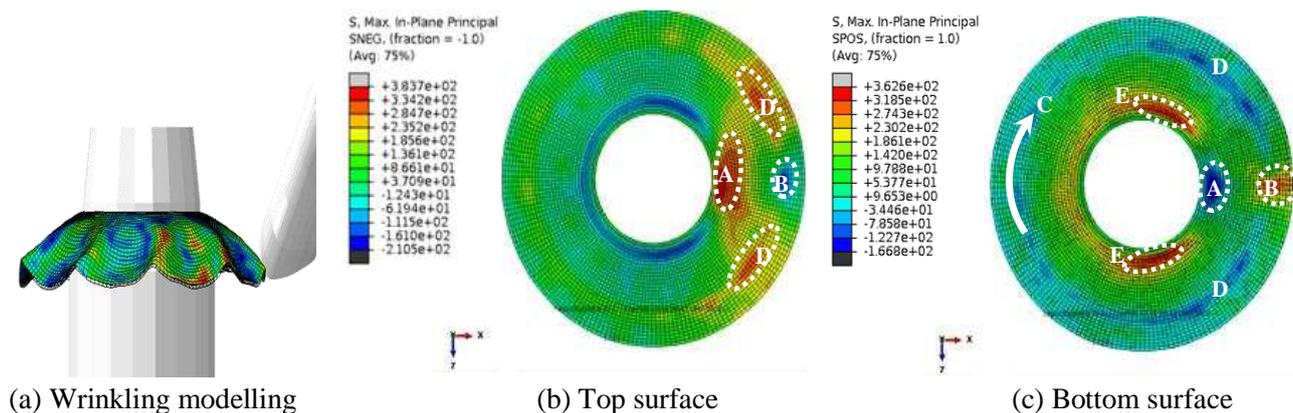
Fig. 7 Maximum in-plane principal stress of top and bottom surface of the blank

5.2 Stress distribution during the development of wrinkling

The development of the tangential stresses on the top and bottom surfaces during the first roller pass, shown in **Fig. 8**, is examined by looking at lines of elements around the circumference in plane with the contact of the roller. **Fig. 9** illustrates the circumference section of the blank under roller contact and the residual bending moments plus bending moments caused by the external force of the roller. At the start of the first pass, the tangential stress distribution is characterised by high bending stresses in the plane of the roller contact ($\theta = 0°$) and low stresses in the rest of the circumferential ring (**Fig. 8a**). In addition to this the top surface away from the plane of roller movement is generally in tension while the bottom surface is in compression, this is consistent with the flange being bent inwards. All of the stresses present are below the material yield stress of 250 MPa. The stress in plane with the roller ($\theta = 0°$) also drops significantly as the direction of travel of the roller changes from into the blank at the start of the pass, to heading more towards the edge of the blank at the end of the pass (**Fig. 8b**). The bending moments at either side of the roller contact ($\theta = 0°$), resisting its motion, increase as the roller nears the edge of the blank as less support can be provided from stiffer parts of the blank nearer the clamped portion to the mandrel.
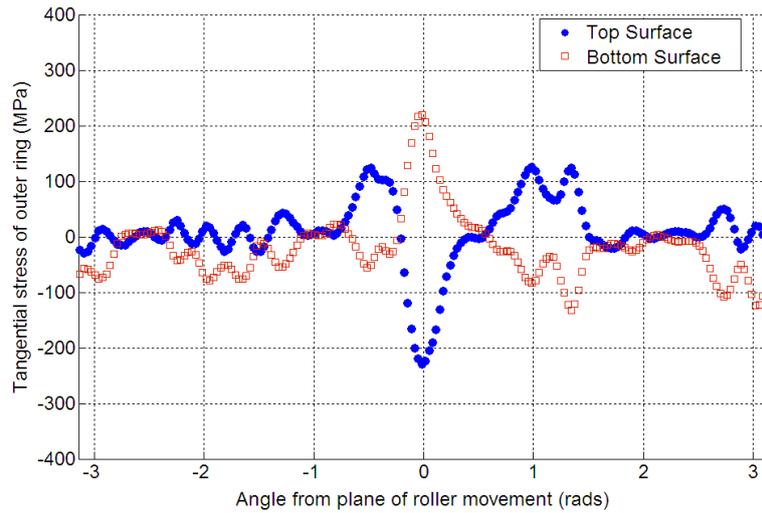
(a) Near the start of first pass
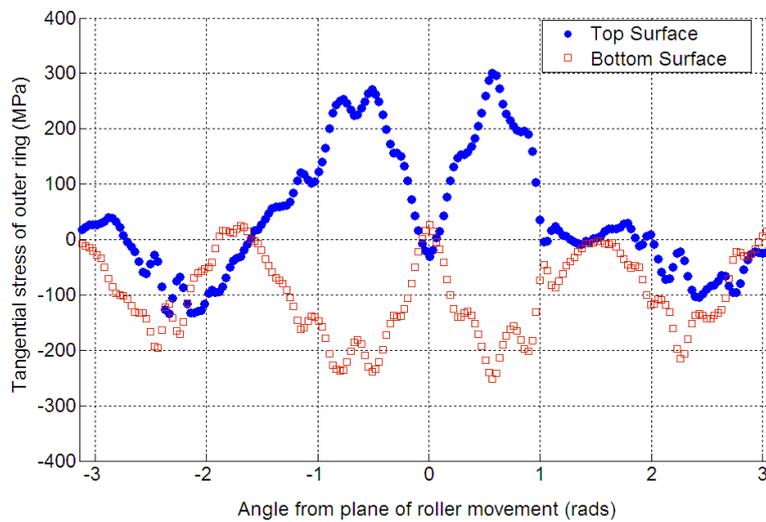
(b) Near the end of first pass

Fig. 8 Distributions of tangential stress on top and bottom surface during the first roller pass
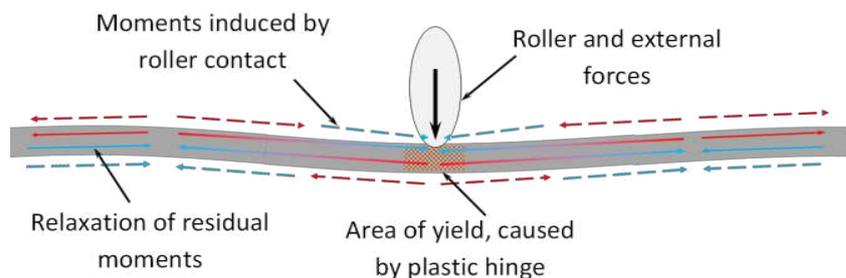
Fig. 9 Illustration of residual moments induced by the roller contact

To examine the stress state of the blank throughout the process of wrinkling, results from three consecutive time frames have been compared in **Fig. 10**. These frames correspond to a moment just before (a), during (b) and just after (c) the appearance of the first wrinkles. The stress distributions in **Fig. 10a** relating to the moment just before wrinkling indicate that the bending stresses in the blank away from the contact have grown such that large compressive and tensile stresses could be observed on the blank on either side of the

roller contact ($\theta = 0°$). The compressive stress away from the roller contact has also risen to around 100 MPa, when comparing with the stresses during the first pass (**Fig. 8a**). In the area affected by the roller contact the characteristic wide resisting moments can be seen again with low tangential stresses in the plane of roller motion ($\theta = 0°$).
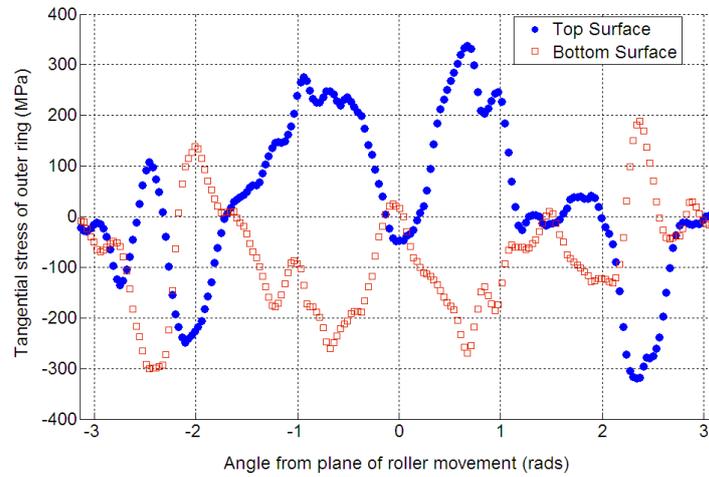
(a) Before the apprearance of first wrinkles

(b) During the apprearance of first wrinkles

(c) Just after the apprearance of first wrinkles

Fig. 10 Tangential stresses at time frames during the appearance of the first wrinkles

Fig. 10b showing the moment of wrinkling must be thought of as a snap shot of a now highly dynamic process. Examination of the displacement plots reveals this time frame relates to the roller passing over what is to become the bottom of a wrinkle. In this situation the plane of roller movement is flanked by residual moments which act to force the section of the blank in plane with the roller downwards. These are relieved by the yielding of the blank in plane with the roller in the form of a plastic hinge, as illustrated in **Fig. 9**. The radial bending stresses caused by flange leaning are also relived. This deformation results in less stress in the blank and therefore less elastic strain, this makes the act of wrinkling energetically favorable. This is confirmed by the effect of wrinkling on the elastic strain energy of the model which is shown in **Fig. 11**.

In the final time frame of stress distributions, shown in **Fig. 10c**, relates to the moment that the top of a wrinkle is passing under the roller, this produces a very different stress pattern to the previous time frame in **Fig. 10b**. Here the supporting moments are very large, this could be due to similar effects as dynamic impact or the feed rate being artificially increased due to the presence of a wrinkle. It can also be seen that the stresses away from the contact are generally lower than the previous time frames due to the formation of wrinkling, shown in **Fig. 10c**. In addition to providing insight into the mechanisms of failure and its causes, this analysis has provided a definite point at which the blank can be said to have wrinkled. The point at which the strain energy indicates that wrinkling is occurring, shown in **Fig. 11**, should be used as the time of material failure of wrinkling, which will be used in the following analysis.
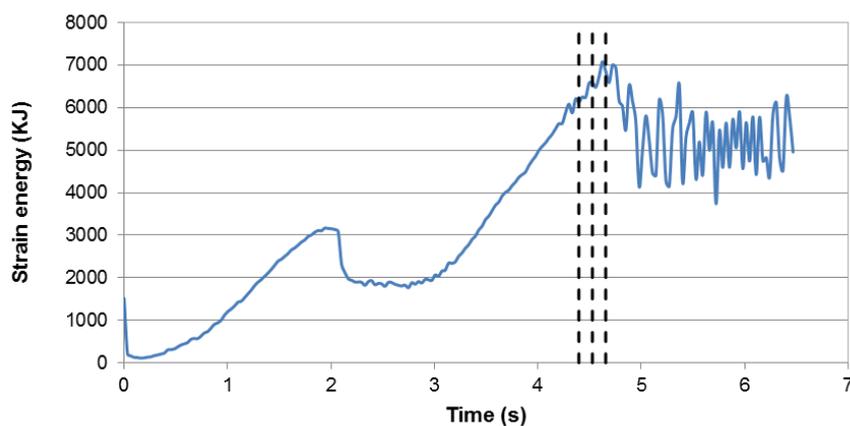
Fig. 11 Elastic strain energy of the 3 time frames examined as indicated by dashed lines.

5.3 Effect of roller path on the initiation of wrinkling

The defining angle of an involute path controls the curvature of the roller path, as shown in **Fig. 4**. As described above wrinkling failure is triggered by the formation of a plastic hinge between the roller and the edge of the blank (**Fig. 9**). If this is the case it is reasonable to assume that when the roller is closer to the edge of the blank the process will be more susceptible to wrinkling failure. During the first pass too low a defining angle will cause equal deformation to the sensitive outer areas of the blank as the inner areas. Too high an angle will force the roller more directly into the blank at the start of the pass causing high bending stresses which could also result in the formation of a plastic hinge.

All models of involute path defined in **Fig. 4** were solved twice each using 4 cores and domains to minimize random computational errors in using domain parallelization. All models failed during the second pass and the time to failure as indicated by the elastic strain energy was recorded. The results for this analysis are shown in **Fig. 12**. The results show that the optimum defining angle for the first pass of this spinning process is around 40°.
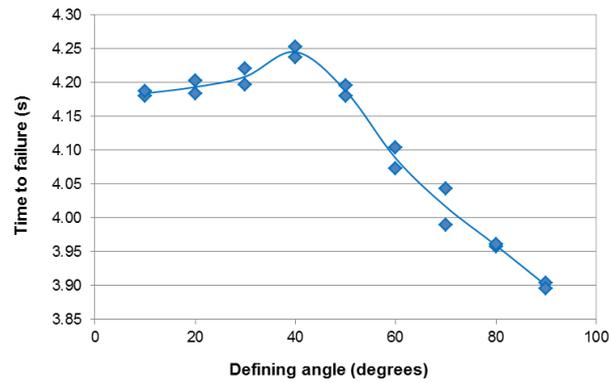
Fig. 12 Defining angle vs. time to wrinkling failure for the involute path models

5.4 Effect of process and material parameters on the initiation of wrinkling

For each parameter investigated, the Box-Behnken design creates 12 pairs of models in which only the parameter of interest varies. The time to failure, defined by a change in the elastic strain energy, of these pairs are compared in order to understand which parameters are most important to the onset of wrinkling failure. In addition to this where an important factor has been found its effect on the process mechanics has been examined.

Increasing the total feed per pass had a negative effect on the time to failure for 10 out of the 12 model pairs, the exceptions being those models with a high blank thickness. Examination of the tangential stress at the edge of the blank, as shown in **Fig. 13**, reveals that for a higher total feed much higher bending stresses exist as supporting moments acting against the roller. Another effect can be seen as the roller nears the edge the blank, the bending stress in plane with the roller movement increases to almost an order of magnitude more for the largest feed per pass compared to the smallest, by comparing two cases given in **Fig. 13**. These larger stresses, particularly those in plane with the roller, will cause wrinkling to occur more quickly and with less previous build-up of residual moments in the blank.
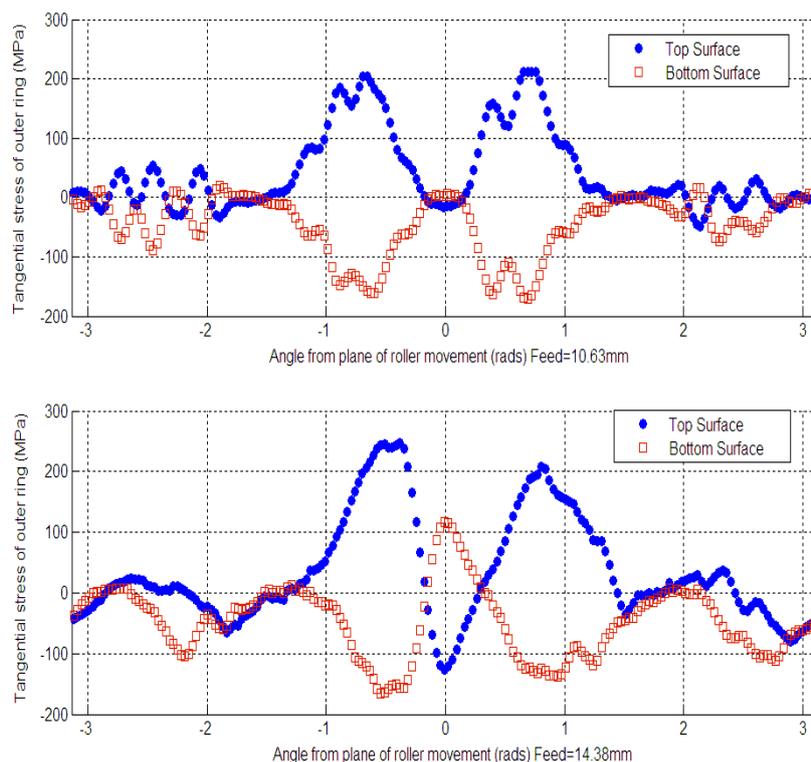
Fig. 13 Effect of roller feed on tangential stress distributions at the end of the first pass

Increasing the feed rate reduces the time to failure for all but 3 model pairs. Similar to the feed per pass, the effect of increasing the feed rate is again to increase the stresses in the material during deformation; however the feed rate could not be shown to have any effect on the bending moments present in the blank between passes.

Increasing the blank thickness increased the time to failure for all but 4 of the 12 model pairs, i.e. the wrinkling trend was reduced as the blank thickness increased. This result is well supported by the literature, concluded by Wang and Long [18], Kleiner et al. [19], Razavi et al. [27]. The edge stress distributions for models of different thicknesses before wrinkling are very similar both during the first pass and between the passes. It is likely that the thinner blank failed more quickly as its plastic moment is smaller than that of the thicker blank with the plastic moment being proportional to the thickness squared. There is more variation in these results than for those of any of the other variables tested. This may be due to the primary mode of deformation changing as the pass progresses; from shear forming when the roller is near the mandrel and the path is steep, to bending when the roller is near the edge of the blank.

The Young's modulus was found to have only a small effect on the stresses during forming, with compressive stresses increasing slightly with the Young's modulus. However, there was a significant effect on the residual stresses in the blank between the passes. The stiffer models typically had much higher residual stresses causing them to collapse into a wrinkled state more quickly, as shown in **Fig. 14**. With a lower yield stress, the blank is able to support less bending stresses and the plastic hinge forms more quickly. This causes the blank to wrinkle. It is possible that for materials of much lower yield stresses the deformation mode will change from large scale bending to local bending/indentation. Increasing the stiffness of the blank material reduced the time to failure. The change of strain hardening exponent value produced almost no change in the time to failure, this is almost certainly due to the fact that these models wrinkled quickly with very little plastic deformation.
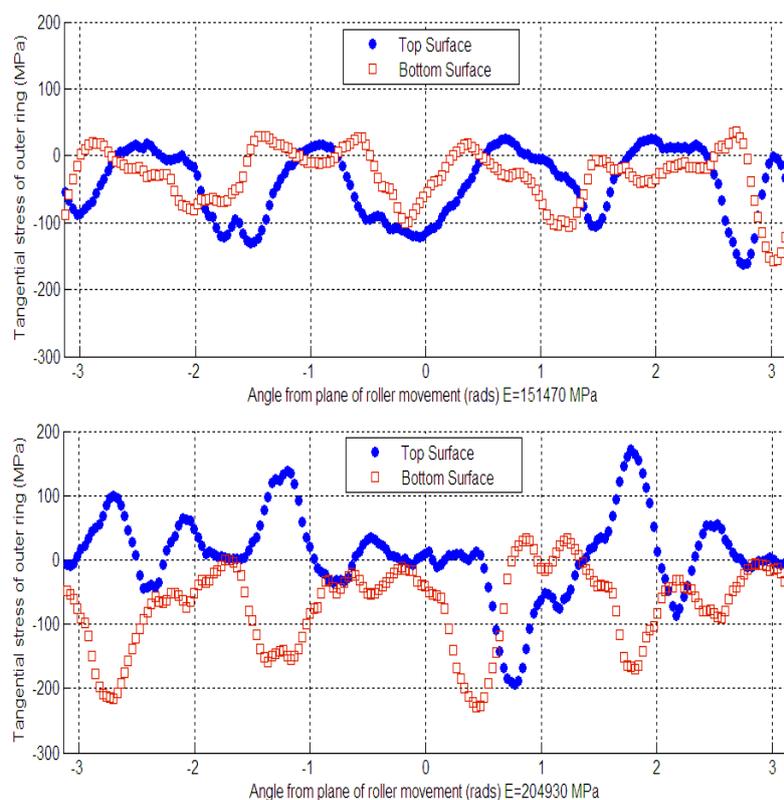
Fig. 14 Effect of Young's modulus on tangential stress distributions at the end of the first pass

6. Conclusions

The initiation of material wrinkling failure and effects of 6 process parameters and material properties were investigated. From the results obtained in this investigation, the following conclusions may be drawn:

Winkling mechanism: It is observed from the FE simulation results that wrinkling instability in conventional metal spinning is caused by the build-up of residual bending moments, with collapse being initiated by the formation of a plastic hinge between the roller and the edge of the blank.

Process parameters: The feed per pass and feed rate produce the most significant effect on the onset of wrinkling as large feeds and high feed rates increase the bending stresses of the blank in plane with the roller contact thus causing the formation of a plastic hinge more rapidly than smaller feeds and feed rates. The involute roller path of an angle of 40 degrees has been found to be optimum for the first roller pass.

Blank thickness: Increasing the thickness of the blank delays the start of material wrinkling due to the fact that the plastic moment is proportional to the thickness squared. This shows that shear deformation is significant in conventional spinning. The amount of variability in response suggests that the main mode of material deformation changes throughout the roller pass.

Material properties: Increasing the yield stress causes slightly higher stresses in the forming area however the blank is able to resist wrinkling for longer. While increasing the Young's modulus of the blank does slightly increase the stresses during the forming process it has a dramatic effect on the magnitude of the residual moments present in the blank. The strain hardening exponent is found to have no significant effect.

References

1. Xia, Q., Xiao, G., Long, H., Cheng, X., Sheng, X. (2014) A review of process advancement of novel metal spinning. International Journal of Machine Tools & Manufacture, 85: 100-121.

2. Runge, M. (1994) Spinning and Flow Forming (D. H. Pollitt, Trans). Leifield, GmbH.

3. Wong, C. C., Dean, T. A., Lin, J. (2003) A Review of Spinning, Shear Forming and Flow Forming Processes. International Journal of Machine Tools & Manufacture, 43: 1419-1435.

4. Music, O., Allwood, J. M., Kawai, K. (2010) A Review of Mechanics of Metal Spinning. Journal of Materials Processing Technology, 210: 3-23.

5. Sebastiani, G., Brosius, A., Homberg, W., Kleiner, M. (2007) Process Characterization of Sheet Metal Spinning by Means of Finite Elements, Key Engineering Materials. 334: 637-644.

6. Wang, L., Long, H. (2011) Investigation of material deformation in multi-pass conventional metal spinning. Materials & Design, 32: 2891-2899.

7. Music O., Allwood, J.M. (2011) Tool-path design for metal spinning. ICTP Special Issue Sheet Metal Forming, the 10th International Conference on Technology of Plasticity, Aachen, Germany.

8. Senior, B.W. (1956) Flange wrinkling in deep-drawing operations. Journal of Mechanics and Physics of Solids, 4, 235-246.

9. Kobayashi S. (1963) Instability in conventional spinning of cones. Journal of engineering for industry, 85(1): 44-49.

10. Kegg, R. (1961) A new test method for determination of spinnability of metals. Journal of Engineering for Industry - Transactions of ASME, 83**:** 118-125.

11. Hayama, M., Tago, A. (1968) The Fracture of Walls on Shear Spinning – Study on the Spinnability of Aluminium Plates, Bulletion of Faculty of Engineering, Yokohama National University, 17: 93-103.

12. Kawai, K., Hayama, M. (1987) Roller Pass Programming in Conventional Spinning by NC Spinning Machine. Advanced Technology of Plasticity, 711-718.

13. Hayama, M., Murota, T., Kudo, H. (1966) Deformation Modes and Wrinkling of Flange on Shear Spinning, Bulletin of JSME, 9(34): 423-433.

14. Hayama, M. (1981) Study on Spinnability of Aluminium and its Alloys. Bulletin of the Faculty of Engineering, Yokohama National University, 30: 63-72.

15. Arai, H. (2003) Robotic Metal Spinning – Shearing Spinning Using Force Feedback Control. Proceedings of 2003 IEEE, International Conference on Robotics & Automation, Taipei, Taiwan, pp. 3977-3983.

16. Xia, Q., Shima, S., Kotera, H., Yasuhuku, D. (2005) A study of the One-path Deep Drawing Spinning of Cups. Journal of Materials Processing Technology, 159: 397-400.

17. Essa, K., Hartley, P. (2009) Numerical simulation of single and dual pass conventional spinning process. International Journal of Material Forming, 2:271–81.

18. Wang, L., Long, H. (2011) Investigation of Effects of Roller Path Profiles on Wrinkling in Conventional Spinning, Proceedings of 10th International Conference on Technology of Plasticity, Aachen, Germany.

19. Kleiner, M., Gobel,R., Kantz, H., Klimmek, Ch., Homberg, W. (2002) Combined Methods for Prediction of Dynamic Instabilities in Sheet Metal Spinning. CIRP Annals-Manufacturing Technology. 51(1): 209-214.

20. Wang, L., Long, H., Ashley, D., Roberts M., White, P. (2011) Effects of the roller feed ratio on wrinkling failure in conventional spinning of a cylindrical cup, Proc. IMechE Part B: J. Engineering Manufacture, 225: 1991-2006.

21. Wang, L., Long, H. (2013) Roller path design by tool compensation in multi-pass conventional spinning, Materials and Design, 46: 645-653.

22. Hamilton, S., Long H. (2008) Analysis of conventional spinning process of a cylindrical part using Finite Element method, Special Edition of Steel Research International, Verlag Stahleisen GmbH, 79(1): 632-639.

23. Liu, C. H. (2007) The simulation of multi-pass and die-less spinning process. Journal of materials processing technology, 192-193: 518-524.

24. Long, H., Wang, L., Jagger, P. (2011) Roller Force Analysis in Multi-pass Conventional Spinning by Finite Element Simulation and Experimental Measurement, Proceedings of The 10th International Conference on Technology of Plasticity, Aachen, Germany.

25. Wang, L., Long, H. (2011) A Study of Effects of Roller Path Profiles on Tool Forces and Part Wall Thickness Variation in Conventional Metal Spinning, Journal of Materials Processing Technology, 211: 2140-2151.

26. Wang, Q., Wang, T., Wang, Z. R., 1989. A Study of the Working Force in Conventional Spinning.

Proceedings of the Fourth International Conference of Rotary Forming, pp. 103-108.

27. Razavi, H., Biglari, F.R., Torabkhani, A. (2005) Study of strains distribution in spinning process using FE simulation and experimental work. Tehran International Congress on Manufacturing Engineering (TICME2005). Tehran, Iran.

Appendix 1: List of model runs for Box-Behnken design

Case Number	Feed per pass (mm)	Feed rate (mm/s)	Yield stress (MPa)	Strain hardening exponent	Thickness (mm)	Young's modulus (MPa)	Time to failure (s)
1	10.625	5.1	250	0.0663	1.4	178200	4.33
2	10.625	5.1	250	0.0897	1.4	178200	4.40
3	10.625	6.9	250	0.0663	1.4	178200	3.51
4	10.625	6.9	250	0.0897	1.4	178200	3.50
5	14.375	5.1	250	0.0663	1.4	178200	4.38
6	14.375	5.1	250	0.0897	1.4	178200	4.37
7	14.375	6.9	250	0.0663	1.4	178200	3.78
8	14.375	6.9	250	0.0897	1.4	178200	3.55
9	12.5	5.1	212.5	0.078	1.19	178200	4.43
10	12.5	5.1	212.5	0.078	1.61	178200	2.04
11	12.5	5.1	287.5	0.078	1.19	178200	1.93
12	12.5	5.1	287.5	0.078	1.61	178200	2.62
13	12.5	6.9	212.5	0.078	1.19	178200	3.00
14	12.5	6.9	212.5	0.078	1.61	178200	3.11
15	12.5	6.9	287.5	0.078	1.19	178200	3.57
16	12.5	6.9	287.5	0.078	1.61	178200	3.64
17	12.5	6	212.5	0.0663	1.4	151470	2.78
18	12.5	6	212.5	0.0663	1.4	204930	3.67
19	12.5	6	212.5	0.0897	1.4	151470	2.79
20	12.5	6	212.5	0.0897	1.4	204930	3.58
21	12.5	6	287.5	0.0663	1.4	151470	4.79
22	12.5	6	287.5	0.0663	1.4	204930	4.01
23	12.5	6	287.5	0.0897	1.4	151470	4.53
24	12.5	6	287.5	0.0897	1.4	204930	4.15
25	10.625	6	250	0.0663	1.19	178200	3.15
26	10.625	6	250	0.0663	1.61	178200	3.90
27	10.625	6	250	0.0897	1.19	178200	3.02
28	10.625	6	250	0.0897	1.61	178200	3.66
29	14.375	6	250	0.0663	1.19	178200	1.93
30	14.375	6	250	0.0663	1.61	178200	2.01
31	14.375	6	250	0.0897	1.19	178200	2.07
32	14.375	6	250	0.0897	1.61	178200	2.00
33	12.5	5.1	250	0.078	1.19	151470	5.71
34	12.5	5.1	250	0.078	1.19	204930	4.44
35	12.5	5.1	250	0.078	1.61	151470	4.77
36	12.5	5.1	250	0.078	1.61	204930	2.35
37	12.5	6.9	250	0.078	1.19	151470	1.67

38	12.5	6.9	250	0.078	1.19	204930	1.59
39	12.5	6.9	250	0.078	1.61	151470	3.22
40	12.5	6.9	250	0.078	1.61	204930	2.32
41	10.625	6	212.5	0.078	1.4	151470	3.57
42	10.625	6	212.5	0.078	1.4	204930	3.28
43	10.625	6	287.5	0.078	1.4	151470	3.68
44	10.625	6	287.5	0.078	1.4	204930	3.66
45	14.375	6	212.5	0.078	1.4	151470	4.16
46	14.375	6	212.5	0.078	1.4	204930	1.34
47	14.375	6	287.5	0.078	1.4	151470	2.00
48	14.375	6	287.5	0.078	1.4	204930	3.55
49	12.5	6	250	0.078	1.4	178200	4.33